PULSED INJECTION TRACER MIXING IN ANNULAR LIQUID FILMS

A. Saxena, J. Eiholzer, and H.-M. Prasser
Laboratory for Nuclear Energy Systems, ETH Zurich
Sonneggstrasse 3, 8092 Zürich, Switzerland
asaxena@lke.mavt.ethz.ch; eijan@student.ethz.ch; prasser@lke.mavt.ethz.ch

ABSTRACT

The functioning of a Boiling Water Reactor (BWR) relies on the effective heat transfer to a multiphase coolant system through a series of different flow regimes along the height of a subchannel and hence, studying such multiphase flow regimes is important with regards to both safety and efficiency. One such type of flow, namely the dispersed vertical annular flow, is present in the uppermost parts of BWR subchannels and is critical in thermal-hydraulics analysis with regards to predicting dryout. Studying the characteristics of such a highly dynamic flow having varied length and time scales requires information through experiments with advanced instrumentation. This work presents a novel experimental technique to study tracer mixing in liquid films in vertical annular flow in a double subchannel geometry using pulsed tracer injection. A conductive tracer is injected into gas driven, de-ionized water film and traced using a liquid film sensor, a high frequency non-intrusive conductivity based sensor. The pulsing is achieved using an electromagnetic contraption wherein a ferromagnetic ball is periodically attracted and released to impact an elastic membrane sealed, tracer filled chamber. The pressure head in the chamber is maintained using a syringe pump in order to achieve similar pulsed volumes of the tracer. Ensemble averaging of multiple injections has been performed to reveal and quantify average flow parameters including mixing coefficients, bulk and interfacial velocity of liquid films. The experiments are conducted with and without a swirl type spacer to quantify the effect of the spacer on the film flow for different gas and liquid flow rates. The current work provides an important insight into the mixing capabilities of spacers, which is important with regards to numerical modeling of vertical annular flow and the prediction of dryout.

KEYWORDS
Dryout, liquid film, annular flow, BWR, mixing

1. INTRODUCTION

Accurate knowledge of heat transfer mechanisms in systems relying on boiling heat transfer is essential for their performance and safety. Annular flow remains a highly relevant class of two phase flow regimes and is important for the operation of several complex systems like nuclear reactors, steam boilers and heat exchangers. Design predictions in such systems are largely made using empirical correlations with lumped parameter models. Lack of reliable experimental data with which to determine model coefficients (e.g. velocity, diffusivity, flow structure) still represents a big source of uncertainty. Some recent advances in novel measurement techniques, for e.g. [1][2], have greatly enhanced the understanding of the physics typically observed in such a highly dynamic flow.

Annular flow is present in the uppermost parts of BWR subchannels with a continuous liquid film covering the fuel rods and steam flowing through the centre of the channels. Each phase can also be transported in the dispersed form with the continuous field of the other phase [3]. The interface is characterized by small amplitude ripple waves along with the large amplitude disturbance waves which are present due to the coupled nature of the two phases. Several authors have identified the importance of periodic disturbance waves in heat transfer prediction in annular flow. Classical models have used turbulent boundary layer theory and mean flow field values to predict liquid film thickness and pressure drop. These have been found to over-predict the heat transfer rate due to the physically different behaviour of the flow.

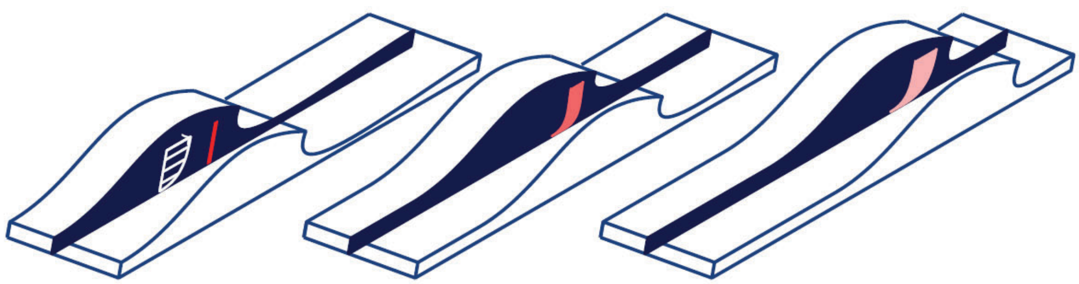

Figure 1. Schematic of mixing of tracer in liquid film

This work reports findings related to the physics of momentum transport in annular liquid films in a double subchannel geometry by tracking and characterizing the movement of tracer particles injected in a pulsed way. This is seen as important with respect to developing accurate heat transfer models to predict the phenomenon of critical heat flux in reactors. Passive scalars are used to aid in the understanding of mixing occurring in flows especially when the complete velocity vector field is unknown. Tracer particles introduced in a flow experiences two things – advection, wherein the cloud of particles advance with the mean flow, and diffusion or dispersion, wherein it spreads with respect to the mean position of the cloud. Due to the process of advection and diffusion, an injected tracer will spread in the flow and will lead to the change of characteristics of a cloud of tracer particles from a state of high concentration and low variance to a state of lower concentration and higher variance.

Theoretical treatment of spreading of tracer particles was done as early as Taylor [4] wherein he adopted a Lagrangian coordinate system traveling at the mean velocity and examined the rate of longitudinal mixing. If a tracer particle is released at a certain location in the flow then after time *t* it will be located at a longitudinal distance *x* from the moving origin where

$$x(t) = \int_{\tau=0}^{t} u'_x(\tau)\,\partial\tau \tag{1}$$

and u'_x = the turbulent velocity fluctuation about the mean. If *N* particles are released then due to the random nature of the turbulent velocity fluctuations they will be at different locations x_i after time *t*. From the conservation of mass principle Taylor stated that the ensemble mean variance of the resulting tracer cloud is identically equal to the mean square displacement of the tracer particles. It was concluded that after a certain time-period when a tracer particle forgets its original velocity, the variance of the tracer cloud increases linearly with time while the rate of this increase depends on the square of the turbulent intensity of the flow. Since this property mirrors that of Fickian diffusion in that the variance of a tracer cloud increases linearly with time, treatment of turbulent diffusion in a stationary homogeneous turbulent flow using Fick's law is often done by the addition of a turbulent diffusion coefficient.

$$\frac{\partial <c>}{\partial t} + <u_x> \frac{\partial <c>}{\partial x} + <u_y> \frac{\partial <c>}{\partial y} + <u_z> \frac{\partial <c>}{\partial z} = (e_m + e_t)\left(\frac{\partial^2 <c>}{\partial x^2} + \frac{\partial^2 <c>}{\partial y^2} + \frac{\partial^2 <c>}{\partial z^2}\right) \tag{2}$$

Turbulent diffusion coefficient, e_t, is related to eddy viscosity through the turbulent Schmidt number Sc_t by -

$$e_t = Sc_t v_t \tag{3}$$

where $\boldsymbol{v_t}$ is the eddy viscosity. When dealing with neutrally buoyant flows, the turbulent Schmidt number is usually around 1.

2. EXPERIMENTS

The adiabatic experiments were performed in a vertical double subchannel flow geometry with a total length of 2.5 meters. The scheme of the facility developed by Damsohn [5] is shown in Fig. 2. Gas is circulated using a side channel compressor since the use of different gases requires a closed loop. Although previous experiments were performed with different gases to study the influence of the properties of the gaseous medium on the film behavior, only air has been used in this work. The liquid is injected through a special slit, 0.5 mm in thickness, directly on the rod geometry. In this way, the liquid flow is injected through an annulus around the rods, which helps developing the film flow faster according to Okada [6]. The water is removed from the gas phase downstream of the test-section in a separator. The temperature of the fluids is kept constant at 20º C using a heat exchanger. The test section has a development length of 70 D. The double subchannel geometry was chosen as the simplest possible geometry still reflecting exchange between two subchannels. This geometry is furthermore still assumed to be sufficient for studying spacer grid influence.

It also allowed to place the electrical film sensor to the surface of the simulator of half of a fuel rod, which made it possible to apply flexible PCB board technology for its manufacturing. The linear dimensions were up scaled by a factor of 2 compared to typical lattice parameters with the intention of a slightly better reflection of governing dimensionless parameters (Re, We) at the high viscosity and surface tension of water at ambient temperature compared to reactor conditions. As a side effect, the bending radius of the PCB board stayed in the acceptable range of 10 mm at the applied fuel rod diameter of 20 mm.

The sensor was placed in the test section so that its lowermost point coincided with the uppermost edge of the spacer. This was done so as to take measurements directly downstream of the spacer. The test section has a square cross section of 50 mm x 50 mm upstream of the water inlet which changes into a double subchannel shaped test section starting from the water injection level. The experiments were conducted at a static pressure of about 1.1 bar at the LFS location with the pressure depending slightly on the velocities of the media.

De-ionized water was used for the liquid film, with a conductivity of around 10 µS/cm to have a low background signal, while a saturated solution of sodium chloride with a conductivity of 100 mS/cm was used as the tracer solution. The spacer, used in this work, is equipped with split vanes to enhance cross flow between subchannels. They have been specifically developed in the context of low quality CHF problems (Shin and Chang [7]). The spacer resembles in geometry to the ULTRAFLOW spacer developed for the ATRIUM fuel assemblies by AREVA (Kraemer et al. [8], Glück [9]).

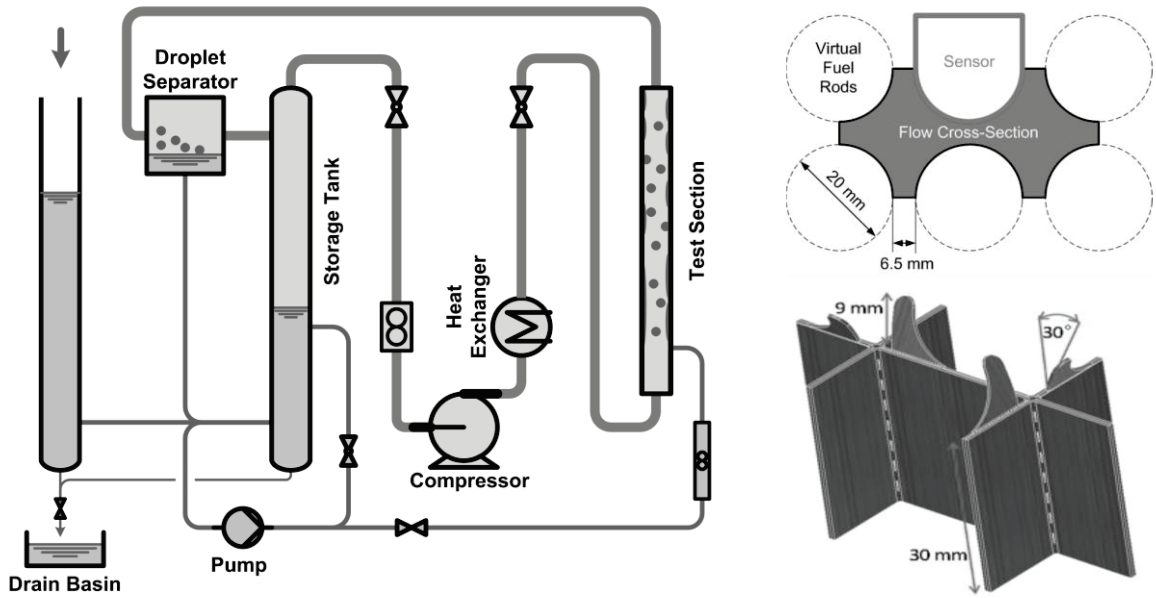

Figure 2. Experimental facility

2.1 Liquid Film Sensor

A conductivity based sensor developed by Damsohn [1], with a 64x16 measurement grid, has previously been used to measure the film thickness around a half rod in the test section. It can also be used to detect changes in conductivity within the liquid film in mixing experiments. The sensor can provide a two dimensional mapping of the conductance at a frequency of 10 KHz. This is seen sufficient to resolve most of the time scales of the disturbances in the liquid film due to the main gas flow. The measuring range of the film thickness varies from 0-800 μm with an accuracy of about 20 μm in the film height direction and a resolution of 2 mm in the longitudinal and lateral directions. The sensor is produced on a flexible multilayer PCB of 0.15 mm thickness. The flexible PCB is bent around a half-cylinder with a 20 mm diameter as shown in Fig 2. The sensor characteristics were calculated by performing potential field simulations for the electrode geometry of the sensor. The sensor has a lower accuracy at the extremities of the half rod due to its construction wherein the first sensing pads are at low distance from the boundary edges.

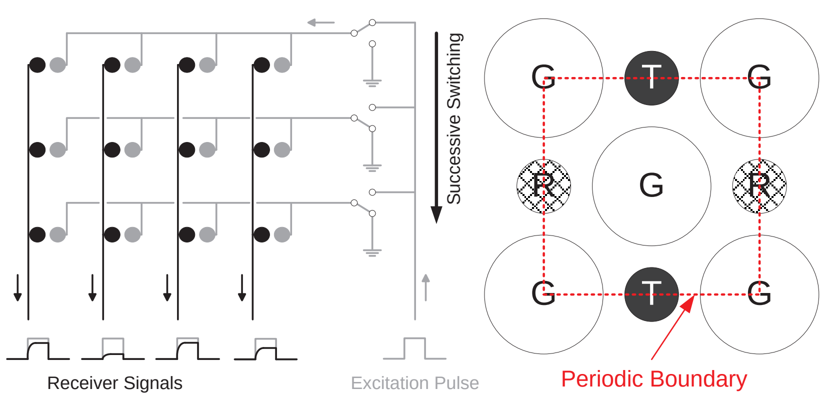

Figure 3. Liquid film sensor

Mixing has been previously studied in this setup with the help of continuous injection of tracer using a syringe pump [10]. This work is expected to add on to the previously obtained knowledge on mixing and momentum transport in liquid films.

2.2 Injection System

To inject small volumes of a conductive tracer, a novel pulsing mechanism operated by an electrical circuit including a pulse generator (PG), transistor and a variable power supply (VPS) was devised. Fig. 5 shows the details of the system. The system works in the following way – a pulsed square wave signal is provided by the pulse generator and amplified using the transistor to supply the current needed to drive the electromagnet (EM). This then attracts or releases the ferromagnetic ball (MB) which acts as a plunger in the hydraulic network of the pumping system. The ejected liquid volume is replenished after a few cycles by the syringe pump to maintain the necessary pressure head. Pulsing duration is controlled by the width of the pulse from the pulse generator.

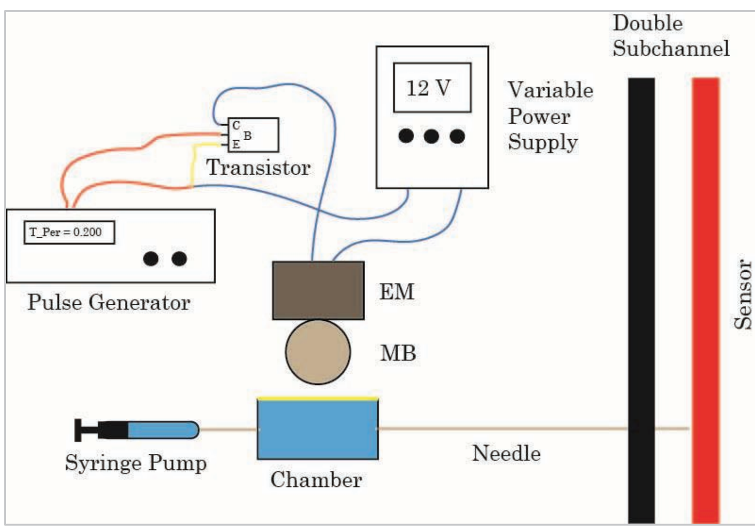

Figure 4. Injection system

2.2.1 Pulsing characteristics

An accurate estimation of flow properties through ensemble averaging depends on the successful injection of an appropriate volume of the tracer. Too high volumes will lead to saturation of the sensor output close to the injection point while too low will result in well mixed regions near the downstream end of the sensor having sensor output comparable to background signal due to waves. The pulsed input signal with a width of 50 ms and a period of 300 ms was provided through the pulse generator. These characteristics were found to give the most desirable output viewed through the data acquisition system. The pulse width includes the traversal time of the ball along with the impact time on the membrane. Knowing the traversal distance q and the deformation of the membrane, the impact time was calculated to be about 10-15 ms. Decreasing the pulse width led to an inadequate amount of tracer being ejected out while increasing it resulted in smearing of the signal at the inlet due to liquid film shear. The period of the pulse was tuned to be long enough so as to avoid overlapping and interference from two successive injections. With the possibility of controlling the distance q, the stiffness of the membrane and the ball mass, the injection mechanism was found to be more robust and economical compared to standard methods of dosing.

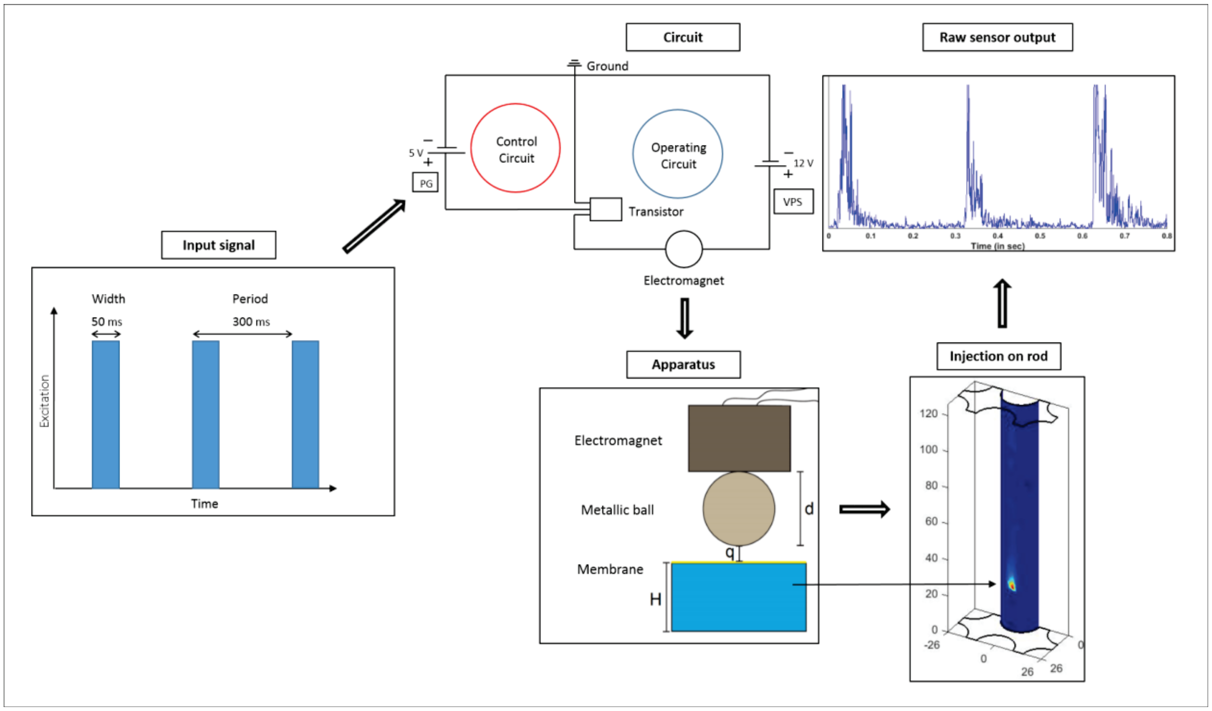

Figure 5. Pulsing characteristics

3. RESULTS

3.1 Ensemble Averaged Tracer Concentration

Measurements are conducted by pulsed injections of tracer particles. Ensemble averaging of data has been done for 200 injection cycles. The injection is made at a distance of 22 mm from the upstream end of the sensor. The injection frame is detected using several filters on the sensor output at the injection pixel. The filters have been chosen so as to avoid counting wavy film structures, spurious or insufficient tracer injection. The data collected by the acquisition system has been post-processed by converting the raw sensor output to normalized concentration mappings over the whole sensor domain. This is achieved by dividing the raw sensor output by the time-averaged background signal of the sensor without the tracer in the flow.

$$S_{norm} = S_{raw}/S_{background} \quad \text{where} \quad S_{background} = S_{film} + S_{systematic\ error} \tag{4}$$

This step not only helped in accounting for different background signal for different flow rates, especially in the presence of a spacer, where the film thickness is a function of the space coordinates, but also for any systematic error in the data acquisition system. Fig. 6 shows the normalized concentration mappings of the advected and diffused tracer cloud as a function of time elapsed after injection. The tracer cloud can be observed to increase in size due to advection and diffusion in the flow. Since the particles are advected at different liquid film velocities, which are dependent on their distance from the wall, the tracer cloud has the appearance of being smeared in the flow direction by the shear flow in the film. Due to the stochastic nature of the flow, the tracer particles also travel at different velocities when injected at different times. Due to the turbulent diffusion in the tangential direction, a concentration flux results in the transport of the particles in the tangential direction as well. Moreover, the sensor has a response curve for conductivity as a function of the distance from it and provides a depth integrated output.

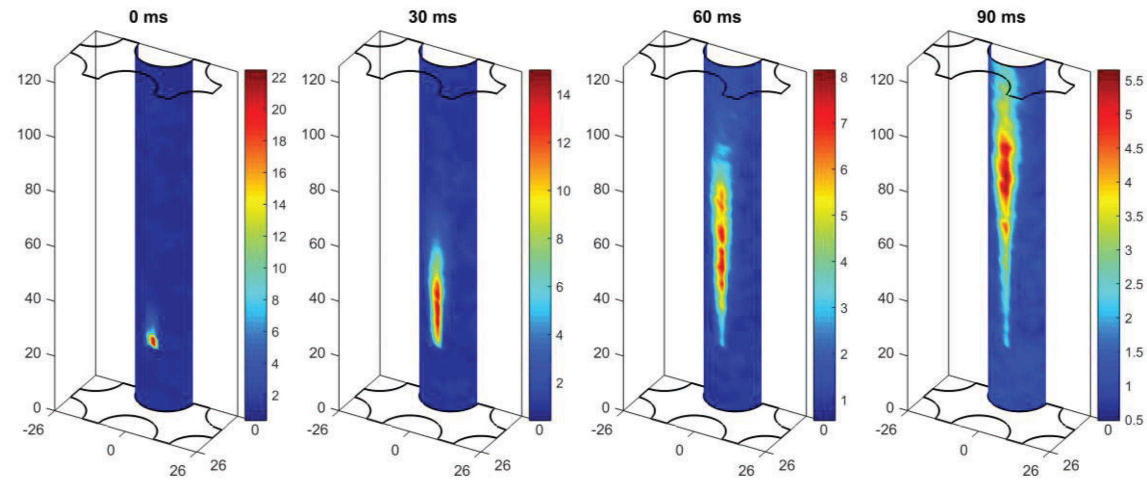

(a)

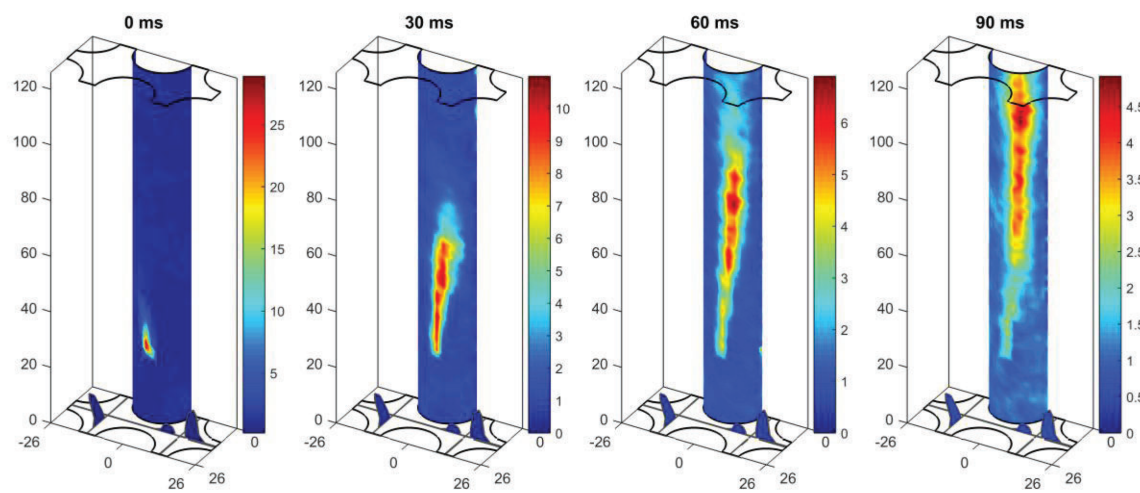

(b)

Figure 6. Normalized concentration mappings of ensemble averaged data a) without spacer and b) with spacer for J_g = 30 m/s and J_l = 0.045 m/s

Hence, a lower concentration region closer to the sensor surface could have an equivalent response compared to a higher concentration region farther away from it. This might explain the multiple peaks observed in the ensemble averaged intensity mappings in Fig. 6. Fig. 6(b) shows the deterministic way in which the particles are advected in the presence of a spacer. The spacer introduces a swirl in the flow resulting in a redistribution of the liquid circumferentially and which naturally leads to a deviation in the tracer trajectory. Estimating the path of the centroid of the tracer cloud gives us the mean trajectory of the particles.

A Gaussian curve was made to fit over the data to obtain information about the width of the pulse along with the centroid. The Gaussian fit was obtained with a confidence interval of 95% over all data points after subtracting the base signal. Fig. 7 shows a cuve fitting over ensemble averaged tracer distribution. A general definition of a Gaussian curve is defined by –

$$y = ae^{-\left[\left(\frac{x-b}{c}\right)^2\right]} \tag{5}$$

where a is the amplitude, b is the centroid and c is related to the peak width. The peaks of the Gaussian curves can be seen to be aligned at the 90^o polar position without any spacers in the flow whereas with them, the peak is markedly shifted from its centered position to close to around 120^o after 80 ms of flow time since injection. The peaks were also observed to decrease in magnitude with time which is expected due to not only turbulent diffusion in the transverse diffusion, as is evident from Fig.7, but also due to axial spreading of the tracer due to flow shear in the liquid film better known as longitudinal dispersion.

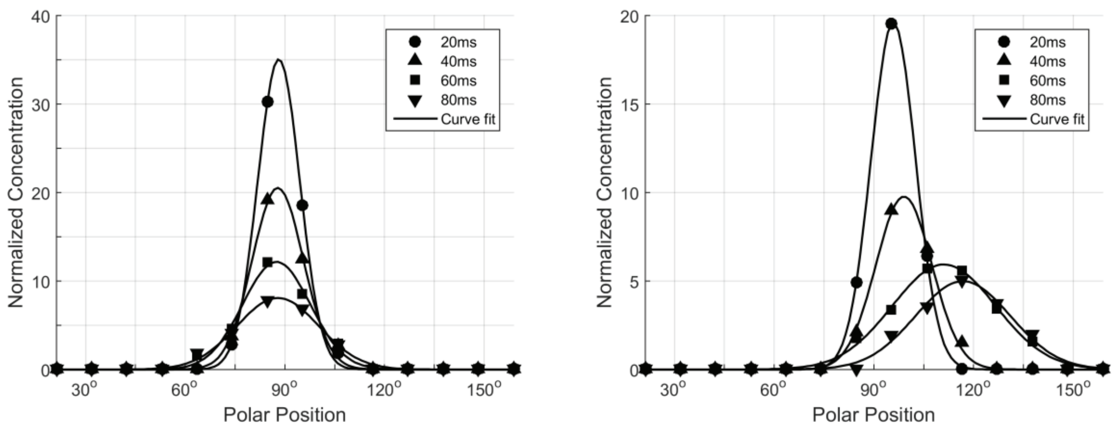

(a) (b)

Figure 7. Centroid and variance estimation of ensemble averaged tracer cloud (a) without spacers and (b) with spacers for J_g = 30 m/s and J_l = 0.04 m/s

In order to estimate transverse diffusion in the liquid film, information about the variance of tracer particles from its mean position is required. Since calculating the width of the tracer cloud by just ensemble averaging the data at discrete intervals of time might not give the right statistics of the behavior of the flow, a better method involves time integrating the normalized concentration for the whole injection cycle and then ensemble averaging for repeated injections. In essence, the width of the tracer cloud at its centroid position might not reveal the real mixing length in the tangential direction and can be distorted from one discrete time frame to the next due to the intermittent features of the flow, for e.g. waves. Time integration alleviates this problem by accounting for this intermittency as all the flow features are registered over the whole flow domain.

Fig. 8. shows the mixing width as a function of the distance from the injection. Due to transverse diffusion of the tracer liquid, the width of the pulse increases with distance downstream. The variance of the tracer particles is found to have a linear trend as a function of distance from the injection point which is expected in homogeneous turbulent flow. For cases without any spacers, the width has an almost constant rate of growth while the absolute magnitude is higher for smaller flow rates. In the presence of spacers, both the growth rate and the absolute magnitude of the width as a function of distance is lower for higher flow rates.

The values are bunched closer together for different flow rates with spacers close to injection due to the alignment of the flow. This trend might be due to lateral velocity components in the gas core that compress the streamlines in the water film via converging shear fields. Therefore, in the presence of spacer grids with vanes, the liquid in the film is not only dispersed in a stochastic way, but is also exposed to lateral components of the time-averaged shear stress. Comparing these parameters of the tracer cloud as a function of distance in the transverse direction should be dealt with caution since it does not take into account any time of flight information. Turbulent diffusivity is further analyzed and calculated in section 3.4.

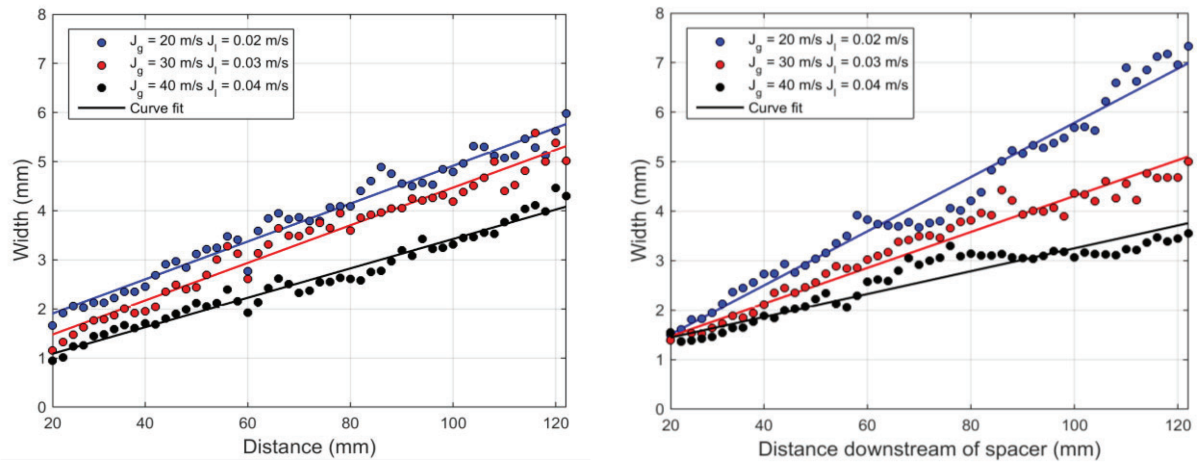

(a) (b)

Figure 8. Tracer cloud width as function of the distance from the injection (a) without spacers and (b) with spacers

3.2 Mean Tracer Trajectory

The mean trajectory of the tracer plume was obtained to get an indication of the effect of the spacer on the flow direction in the film. The path was found by plotting the centroid of the time-integrated, ensemble averaged tracer data, which was obtained from the parameter b in Eq. 5, as a function of distance downstream of injection. Except for some fluctuations that are explained by the turbulence in the gas core, the tracer travels in a straight line in the absence of a spacer, while the spacer vanes cause a deterministic lateral displacement. As mentioned in the previous section, it can be seen in Fig. 9 that the liquid flow is aligned in a deterministic way close to the spacer which is independent of the gas and liquid flow rates and is dependent on the spacer vane angle.

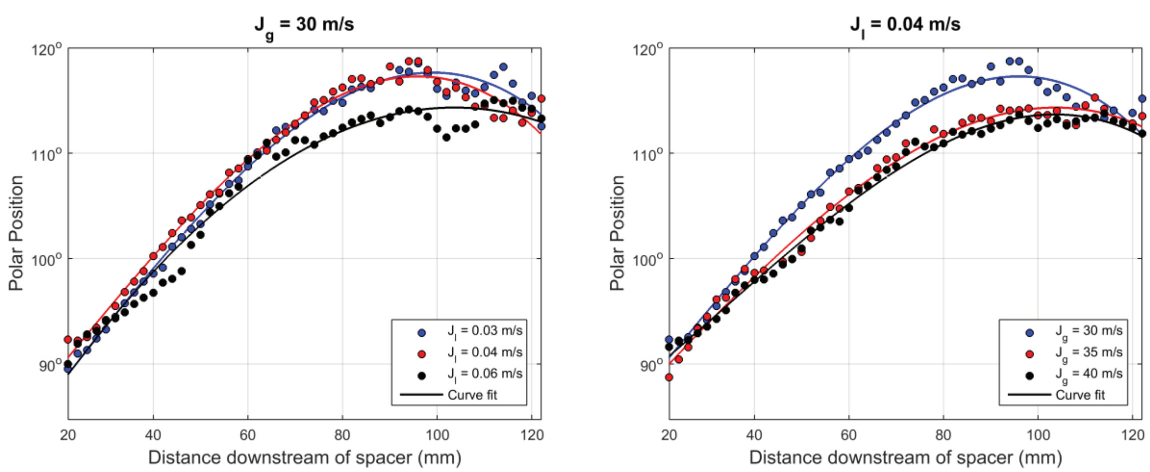

(a) (b)

Figure 9. Trajectory of centroid of tracer cloud

Comparing the trajectory for different liquid flow rates in Fig. 9(a), a smaller deviation from a straight line path can be observed for $J_l = 0.06$ m/s. This could be due to the larger role played by inertia for higher liquid flow rates, hence forcing the tracer to follow a straighter path and delaying the transverse movement induced by the spacer. Gas flow seems to have a similar effect as is evident in Fig. 9(b) where a smaller gas flow rate induces a larger transverse movement.

3.3 Velocity Measurement

3.3.1 Bulk velocity estimation

The bulk velocity, $\mathbf{V_b}$, estimated here is defined as the space average (in the flow direction) of the depth averaged velocity of the liquid film. Since the bulk of the tracer can be assumed to be advected with the bulk velocity of the liquid film, tracking the movement of the centroid of tracer cloud and finding its spatial shift after a certain time period Δt gives the bulk velocity by –

$$\mathrm{V}_b = (\Delta \mathrm{x}_{centroid}^2 + \Delta \mathrm{y}_{centroid}^2)^{1/2} / \Delta \mathrm{t} \tag{6}$$

The centroid of a cloud is found by –

$$\mathrm{x}_{centroid} = \int_1^{N_x} \mathrm{x}.\,\mathrm{S_x} dx \Big/ \int_1^{N_x} \mathrm{S_x} dx \quad \text{and} \quad y_{centroid} = \int_1^{N_y} \mathrm{y}.\,\mathrm{S_y} dy \Big/ \int_1^{N_y} \mathrm{S_y} dy \tag{7}$$

where N_x and N_y are the number of data points in x and y direction respectively, and $\mathrm{S_x}$ and $\mathrm{S_y}$ are the sum of normalized concentration values along a row and column of the sensor respectively. Fig. 10 shows the bulk liquid film velocity averaged from the injection point to 100 ms of flow time with Δt = 10ms. $\mathbf{V_b}$ can be observed to increase with increasing both J_l and J_g.

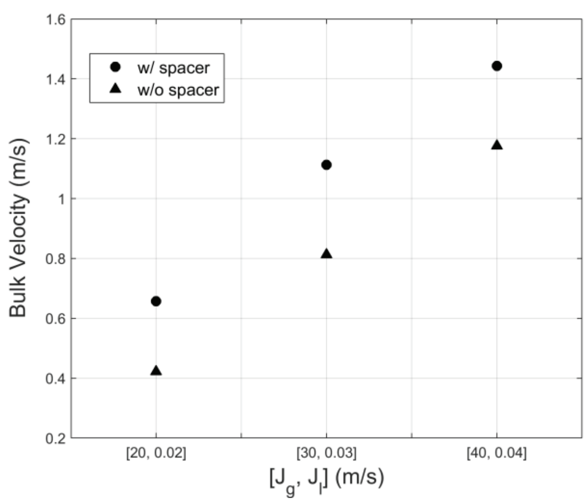

Figure 10. Bulk velocity of film with and without spacers

The bulk velocity is found to increase in an almost linear trend for both with and without spacers. Since $\mathbf{V_b}$ estimated here is along the pathline of the mean motion of the tracer particles, where a higher local liquid flow rate occurs due to the alignment of the flow by the spacers, it is expectedly higher compared to the case without spacers. A nearly constant increase in the bulk velocity values is also observed when spacers are present.

3.3.2 Average interfacial velocity estimation

The average interfacial velocity, $\mathbf{V_i}$, estimated here, is defined as the ensemble averaged velocity of the fastest moving layer of the liquid film and is space averaged over the flow domain in the axial direction. This is not to be confused with the velocity of the waves but is rather an ensemble averaged velocity of the top layer of film which includes the effect of waves and the fastest substrate layer. This was calculated by tracking the movement of the front of the tracer cloud as shown in Fig.11 and finding its spatial shift Δx_{front} after a certain time period Δt.

$$V_f = (\Delta x_{front}^2 + \Delta y_{front}^2)^{1/2}/\Delta t \quad (8)$$

The cloud front is taken to be an iso-contour of the normalized concentration mappings. A value of 1.5 has been chosen which correlates to a concentration with a conductance value 150% of the time-averaged background signal without any tracer. This procedure is restricted to 50 ms of flow time to clearly distinguish between the regions with and without the tracer. At large times after injection, the tracer becomes well mixed near the downstream end of the sensor especially in the presence of spacers, which leads to difficulties in demarcating the separate regions.

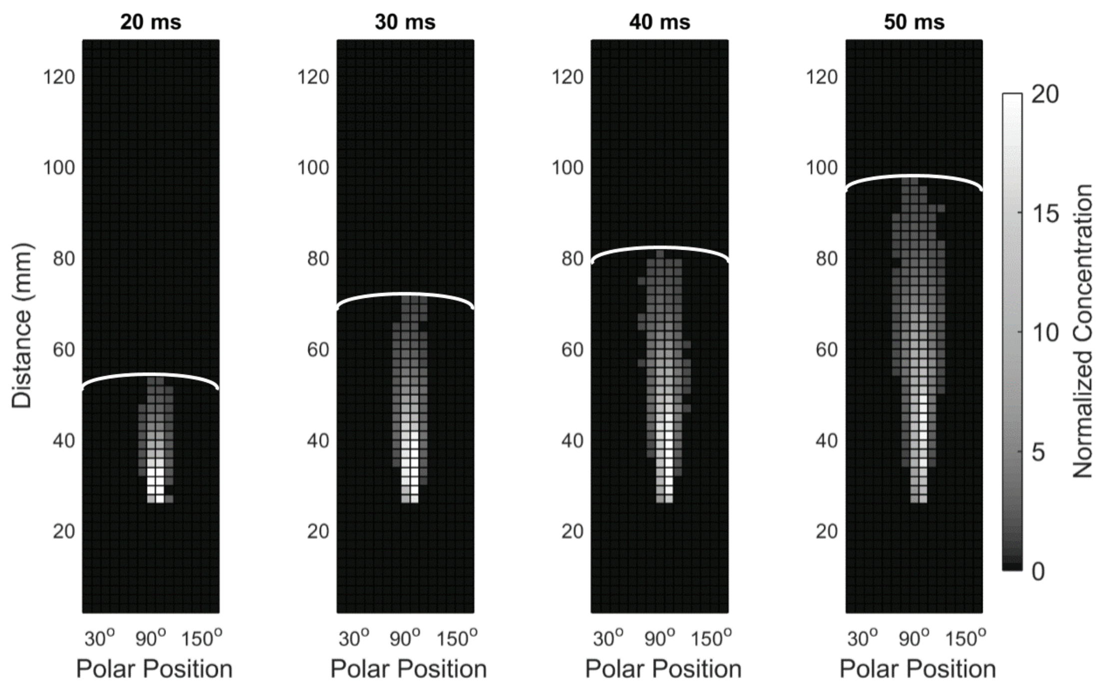

Figure 11. Cloud front tracking for J_g = 30 m/s and J_l = 0.045 m/s

Even though the tracer cloud front might diffuse downstream of the injection point from a sharp front due to axial diffusion of concentration, velocities calculated by tracking an iso-contour is expected to give only slight errors for $\mathbf{V_i}$ due to the high Peclet numbers found in the flow. Fig. 12 shows the interfacial velocity averaged from the injection point to 50 ms with Δt = 10ms. Fig. 12(a) shows the comparison of $\mathbf{V_i}$ with and without spacers. As might be expected, higher values are found in the cases with spacers due to the effect of deterministic gas shear fields. Fig. 12(b) compares $\mathbf{V_i}$ and $\mathbf{V_b}$ for different J_g and J_l and reveals that the difference between them decreases for higher flow rates. This might be due to the increase in mixing in the top layers of the liquid film. Since waves are essentially large masses of turbulent liquid flow, their larger effect can be attributed to higher wave frequency and larger amplitudes for higher flow rates and could be the cause of higher mixing. This also underlines the fact that the velocity profile in the liquid film departs from a laminar velocity profile since the difference between the interface and the bulk velocity should increase with the bulk velocity rather than the opposite found here.

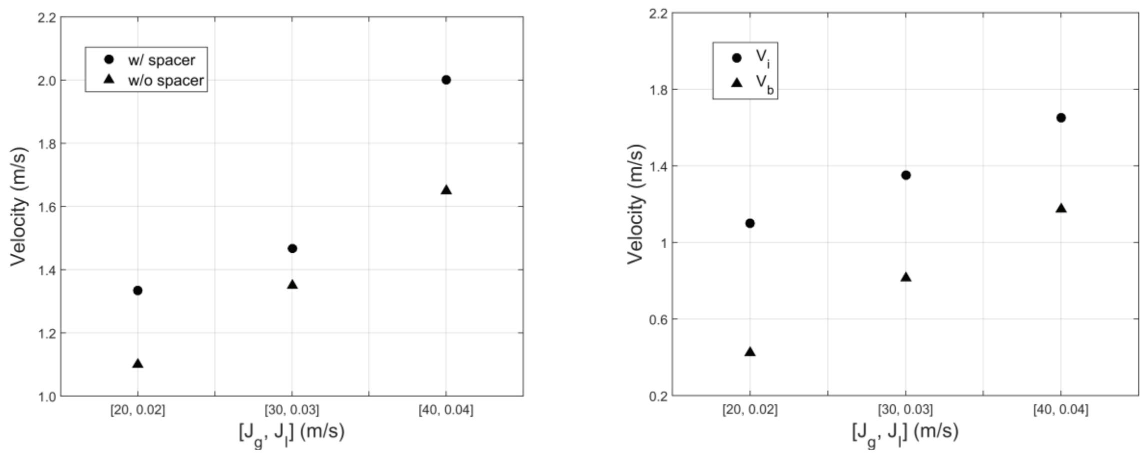

(a) **(b)**

Figure 12. (a) Comparison of average interfacial velocity (V_i) and (b) comparison of bulk velocity (V_b) and average interfacial velocity (V_i) without spacer

Since the average interfacial velocity is more than twice the bulk velocity for J_g = 20 m/s and J_l = 0.02 m/s, it can be postulated that the momentum transfer in the top layers of the liquid film is governed mostly by the gas side shear through the interface. As the flow rates are increased, the interactions of the interface with the gas side turbulence might generate turbulent structures in the liquid film which transfer the high axial momentum from the top layers towards the bulk of the liquid film. This is in line with the surface renewal theory proposed by Komori et.al [12] who attributed the mixing in the liquid side to downwards bursts. Further analysis is required to make more assertions about momentum transport in liquid films. Damsohn [5] and Saxena [10] both independently found the wave velocities to be several times higher than the bulk velocities in this work which might contribute substantially to mixing in liquid films.

3.4 Estimation of Turbulent Diffusivity

To calculate the turbulent diffusivity in the tangential direction, a method developed by Roberts [11] based on the space variance of the measured concentration is used. A space averaged transverse diffusion coefficient is calculated through the change of the variance with time

$$e_t = \frac{1}{2}\frac{\partial\sigma^2}{\partial t} = \frac{1}{2}\frac{\partial\sigma^2}{\partial x}.\frac{\partial x}{\partial t} \approx \frac{1}{2}\frac{\partial\sigma^2}{\partial x}.V_b \tag{9}$$

where σ^2 is the variance from the Gaussian fit , x is the axial direction while V_b is the bulk liquid film velocity estimated from section 3.3.1 to convert the axial distance in a time-of-flight. Fig. 13 gives the results of the transverse turbulent diffusivity with and without the presence of the spacers.

Interestingly, the transverse turbulent diffusivity (**e_t**) gets enhanced in the presence of the spacer only for the first two data points but is lower for J_g = 40 m/s and J_l = 0.04 m/s compared to the case without spacers. The spacer is actually less efficient in mixing for this higher gas and liquid superficial velocity. Even though the bulk velocity is higher when the spacers are present, the transverse spatial variance is lower compared to the case without spacers. The suspected reason could be the imposition of high mean shear field by the large gas flow which may counteract the process of diffusion directly downstream of the spacer. Since this value is an average over the flow domain of the sensor, it very well may be that an increase in turbulent diffusivity is found further downstream of the sensor. The values found in this experimental study are by orders of magnitude higher than the molecular diffusion coefficient of salt (NaCl) in water ($\approx 10^{\wedge(-9)}$ m^2/s). The increasing value of turbulent diffusivity in the liquid film without spacer and with increasing gas and liquid flow rates also suggests the increasing turbulent intensities due to both gas side interfacial shear and wall generated turbulence. At this point of time their individual effect on mixing is not straightforward and clear. The effect of droplets on the scalar transport is captured implicitly through its dependence on the flow velocity field.

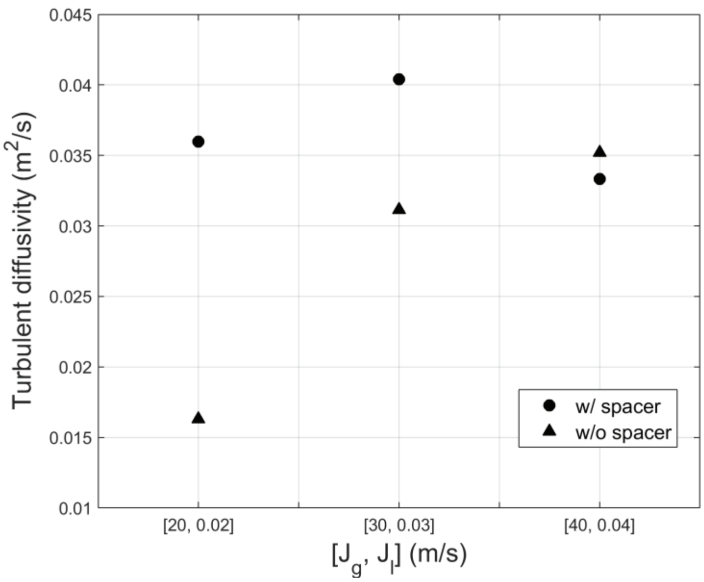

Figure 13. Comparison of transverse turbulent diffusivity with and without spacers

4. CONCLUSION

Experiments have been carried out to study diffusion and advection in liquid films driven by gas shear as part of two-phase annular flow in a double subchannel geometry in adiabatic conditions. A highly conductive tracer was injected directly in deionized water film and traced using a conductivity based sensor. By repeating and recording multiple injections of the tracer in the film, mean and variance of the tracer trajectory has been estimated. Bulk liquid film velocity has been found by tracking the mean tracer position over discrete time intervals while the average interfacial velocity has been estimated by establishing the cloud front and tracking it over discrete time intervals. Evidence has been found to suggest departure from a laminar velocity profile in the liquid film with increased vertical mixing for higher gas and liquid flow rates.

Furthermore, the effect of a swirl-type spacer grid on the flow field has been found to cause circumferential velocity and shear stress components leading to a redistribution of the liquid flow rate across the rod from its steady state. Absolute magnitude of the turbulent diffusivity has been found to be several orders of magnitude higher compared to the diffusion coefficient of salt (NaCl) in water indicating the enhancement of diffusion due to turbulent nature of the flow. Although turbulent diffusivity is found to increase downstream of spacers for some gas and liquid flow rates compared to when no spacers are present, it is also found to be lower for the highest gas and liquid flow rate case indicating reduced mixing in liquid film directly downstream of spacers.

This work lays out a novel method in estimating flow properties in liquid films which are part of gas-driven vertical annular flow and helps to characterize the nature of mixing with and without the presence of spacers in BWR channels.

NOMENCLATURE

D	Hydraulic diameter (m)
J_g	Superficial gas velocity (m/s)
J_l	Superficial liquid velocity (m/s)
e_t	Turbulent diffusion coefficient
v_t	Eddy viscosity (m^2/s)
Sc_t	Turbulent Schmidt number (m^2/s)
S_{norm}	Normalized concentration
V_b	Bulk film velocity (m/s)
V_i	Average interfacial velocity (m/s)
σ^2	Variance of Gaussian fit

REFERENCES

1. M. Damsohn, H.-M. Prasser, "High-speed liquid film sensor for two-phase flows with high spatial resolution based on electrical conductance", *Flow Measurement and Instrumentation,* **Volume 20** (Issue 1), (2009).
2. H-M. Prasser, A. Böttger, and J. Zschau, "A new electrode-mesh tomograph for gas–liquid flows", *Flow measurement and instrumentation*, 9(2), pp. 111-119 (1998).
3. B. J. Azzopardi, "Drops in annular two-phase flow", *International Journal of Multiphase Flow*, 23, pp. 1-53 (1997).
4. G. I. Taylor, "Diffusion by continuous movements", *Proceedings of the London Mathematical Society*, 2(1), pp. 196-212 (1922).
5. M. Damsohn, H.-M. Prasser, "Experimental studies of the effect of functional spacers to annular flow in subchannels of a BWR fuel element", *Nuclear Engineering and Design*, **Volume 240 (**Issue 10), (2010).
6. O. Okada, H. Fujita, "Behavior of liquid films and droplets in the non-equilibrium region of a downward annular mist flow (comparison of porous and central nozzle mixing methods)", *International Journal of Multiphase Flow,* **Volume 19 (**Issue 1), (1993).
7. B. S. Shin, S. H. Chang, "CHF experiment and CFD analysis in a 2x3 rod bundle with mixing vane", *Nuclear Engineering and Design*, **Volume 239** (Issue 5), (2009).
8. W. Kraemer, G. Proebstle, W. Uebelhack, T. Keheley, K. Tsuda, S. Kato, "The ULTRAFLOW spacer—an advanced feature of ATRIUM fuel assemblies for boiling water reactors", *Nuclear Engineering and Design*, **Volume 154** (Issue 1), (1995).
9. M. Glück, "Validation of the sub-channel code F-COBRA-TF: Part I. Recalculation of single-phase and two-phase pressure loss measurements", *Nuclear Engineering and Design,* **Volume 238** (Issue 9), (2008).
10. A. Saxena, J. Sanchez and , H.-M. Prasser, "Transverse Mixing in Annular Liquid Film in BWR Subchannel with Spacers", *The 10th International Topical Meeting on Nuclear Thermal-Hydraulics, Operation and Safety (NUTHOS-10)*, Okinawa, Japan, December 14–18, (2014).
11. Roberts, J.W. Philip, R.W. Donald, "Turbulent diffusion", *Environmental Fluid Mechanics–Theories and Applications*, pp. 7-45, (2002).
12. S. Komori, R. Nagaosa, Y. Murakami, "Turbulence structure and mass transfer across a sheared air–water interface in wind-driven turbulence", *Journal of Fluid Mechanics*, 249, pp 161-183 (1993)